Final Technical Report on "Laboratory Investigation of Contact Freezing and the Aerosol to Ice Crystal Transformation Process"

Based on tasks supported by the Atmospheric System Research program (DOE Office of Biological and Environmental Research), DOE Award Number DE-SC0006949

PI: R. A. Shaw[1]; Other involved personnel and collaborators: N. Black[1], J. Charnawskas[1], C. Gurganus[1], A. Laxo[1], M. Ovchinnikov[2], F. Stratmann[3], F. Yang[1]

[1] Atmospheric Sciences Program and Department of Physics, Michigan Technological University
[2] Pacific Northwest National Laboratory
[3] Institute for Tropospheric Research, Leipzig, Germany

Covering the period September 2011 - September 2014

Address of recipient organization:
Michigan Technological University
1400 Townsend Drive
Houghton, MI 49931
USA

Table of Contents:

1. Overview of Accomplishments

This project has been focused on the following objectives: 1. Investigations of the physical processes governing immersion versus contact nucleation, specifically surface-induced crystallization; 2. Development of a quadrupole particle trap with full thermodynamic control over the temperature range 0 to –40 °C and precisely controlled water vapor saturation ratios for continuous, single-particle measurement of the aerosol to ice crystal transformation process for realistic ice nuclei; 3. Understanding the role of ice nucleation in determining the microphysical properties of mixed-phase clouds, within a framework that allows bridging between laboratory and field measurements.

Personnel over the course of the project have included the PI, Prof. Raymond Shaw, three graduate students, and two undergraduate students:

- Nicholas Black, who completed a M.S. in Physics in summer 2013 based on his work with the quadrupole trap.
- Colin Gurganus, who completed a Ph.D. in Atmospheric Sciences in early fall 2014 and who was supported by a DOE Graduate Research Fellowship. Mr. Gurganus' research involved the substrate nucleation experiments described in this report.
- Fan Yang, an Atmospheric Sciences Ph.D. student who started work on this project in August 2012, having come to us with a M.S. in Atmospheric Sciences from Peking University. Mr. Yang's work involves studies of ice nucleation and microphysics in mixed-phase, stratiform clouds.
- Two undergraduate students, Joseph Charnawskas and Adam Laxo, have been involved with the substrate nucleation experiments during 2013 and 2014, respectively, as the basis of their senior research projects required for a B.S. in Physics. Mr. Charnawskas has since joined the group of Prof. Daniel Knopf at SUNY Stony Brook as a graduate student, and Mr. Laxo is currently applying for graduate studies in Atmospheric Sciences.

In addition, Dr. Mikhail Ovchinnikov from Pacific Northwest National Laboratory and Dr. Frank Stratmann from the Leibniz Institute for Tropospheric Research have played active roles in collaborating on the project.

The project has led to the following publications:

Gurganus, C., A. B. Kostinski, and R. A. Shaw, 2011: Fast imaging of freezing drops: No preference for nucleation at the contact line. *J. Phys. Chem. Lett.*, 2, 1449−1454.

Gurganus, C., A. B. Kostinski, and R. A. Shaw, 2013: High-speed imaging of freezing drops: Still no preference for the contact line. *J. Phys. Chem. C*, **117**, 6195-6200.

Gurganus, C. W., J. C. Charnawskas, A. B. Kostinski, and R. A. Shaw, 2014: Nucleation at the contact line observed on nano-textured surfaces. *Phys. Rev. Lett.*, accepted for publication (preprint available at http://arxiv.org/abs/1410.7640).

Yang, F., M. Ovchinnikov, and R. A. Shaw, 2013: Minimalist model of ice microphysics in mixed-phase stratiform clouds. *Geophys. Res. Lett.*, **40**, 1-5.

Yang, F., M. Ovchinnikov, and R. A. Shaw, 2014: Microphysical consequences of the spatial distribution of ice nucleation in mixed-phase stratiform clouds. *Geophys. Res. Lett.*, **41**, 5280-5287.

2. Substrate Nucleation Experiments

The notion of surface crystallization has come into focus recently as a potentially important pathway for both homogeneous and heterogeneous freezing of water. We have carried out experiments in an environmental control chamber in which we use a high speed camera to image water drops freezing on a substrate. Experiments performed on an idealized, uniform silicon substrate are described in Section 2.1, and then the newly developed environmental control chamber that allows for the use of more complex substrates, as well as for a side camera view, is described in Section 2.2. Experiments on substrates with controlled textures are described in Section 2.3.

2.1 Contact-Line Versus Interfacial-Plane Experiments

We have conducted a series of experiments using high speed imaging of supercooled water drops to study the phenomenon of surface crystallization. Our geometry avoids the "point-like contact" of prior experiments by providing a simple, symmetric contact line (triple line defined by the substrate-liquid-air interface) for a drop resting on a homogeneous silicon substrate. Furthermore, the imaging configuration localizes nucleation sites in the horizontal plane so that their spatial distribution can be examined directly for possible preference near the contact line. Additionally, by using low cooling rates and avoiding substrate cooling, our design minimizes temperature variation within the water drop. The 189 freezing events display nearly perfect spatial uniformity in the immersed (liquid-substrate) region and, thereby, no preference for nucleation at the triple line. This is in contrast to prior experiments where a strong preference for surface freezing (in the contact mode) was observed. The results are explained in more detail in the following figures and their captions, as well as in the paper: Gurganus, C., A. B. Kostinski, and R. A. Shaw, "Fast imaging of freezing drops shows no preference for nucleation at the contact line." *J. Phys. Chem. Lett.*, 2, 1449-1454 (2011).

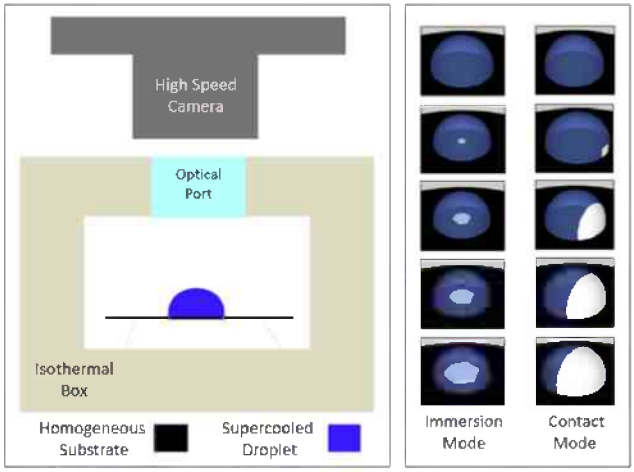

Figure 2.1: Experimental design and nucleation geometry. Left Panel: Schematic side view of the experimental setup. The high speed camera is configured to pinpoint locations of freezing events on the substrate. The drop rests on a clean homogeneous and isothermal silicon wafer. The droplet and substrate are encased in an isothermal box and the walls cool slowly, thereby minimizing temperature gradients. Right Panel: Schematic perspective view of two freezing drops, illustrating an interior substrate event (immersion mode) and an event occurring at the triple line (contact mode).

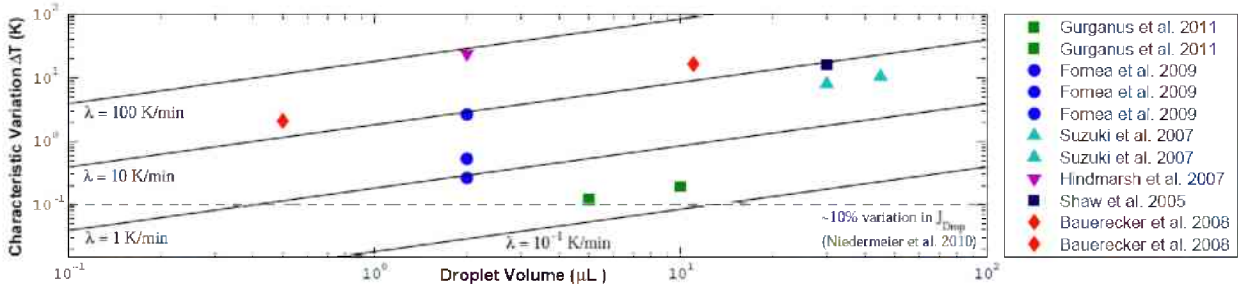

Figure 2.2: Deviation from thermal homogeneity (equilibrium) within drops, subjected to steady cooling. Here we present likely thermal variations ΔT for various experiments, estimated on the basis of thermal relaxation time τ and applied cooling rate λ. The thermal relaxation time is estimated using a characteristic length scale $V^{1/3}$ (for aspherical drops). Contours of the experimental control parameter λ are also shown. Points are shown for the conditions of various relevant experiments; citations are available in the published paper.

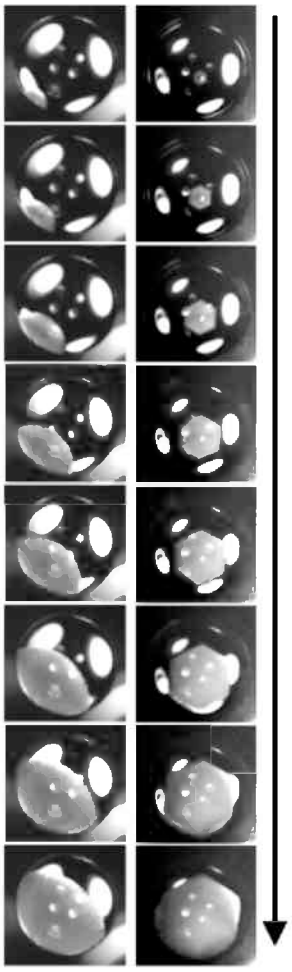

Figure 2.3: Progressions (time evolves downward) of contact (left) and immersion (right) nucleation events for a 10μL spherical cap droplet, viewed from above. The images have been enhanced for contrast, with the freezing front appearing in grey and very bright LED reflections evident. In the immersion film, the nucleated crystal is oriented with the basal plane, aligned with the imaging plane, thereby showing a hexagonal shape, but this is not necessarily the preferred orientation. These videos were recorded at 20,000 frames per second, with every 20^{th} frame displayed (0.001s time steps between images).

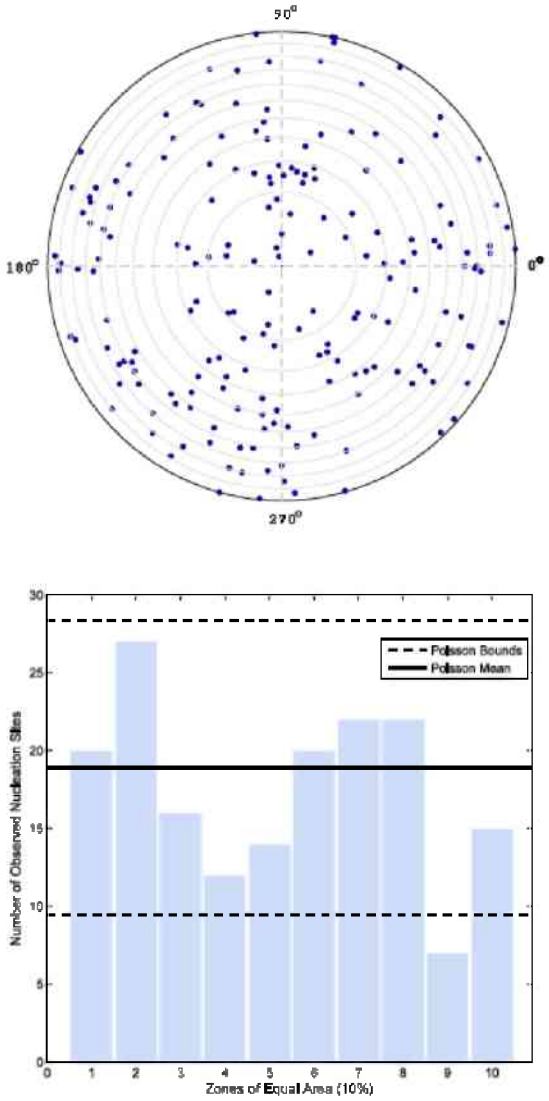

Figure 2.4: Evidence for spatial uniformity of nucleation events. Contrary to expectations, there is no preference for perimeter (contact mode) nucleation. Top panel: locations of the 189 freezing events on the horizontal plane. Radial positions have been scaled by drop radius to facilitate comparison between runs. Bottom panel: Equal area histogram of 10 circular bands provides a quantitative measure of spatial uniformity. The solid horizontal line denotes the expected number of events per bin (19) assuming uniform distribution, and the dashed horizontal lines mark the Poisson bounds.

2.2 Development of New Environmental Control Chamber

A new chamber was developed and tested, with the aim of allowing for both top and side viewing of test droplets, and to allow more flexibility in the experiments. For example, experiments with surface-etched substrates and with a piezoelectric IN-probe are currently underway. The chamber, shown in Figure 2.5, is designed in three sections, with the top and bottom regions actively cooled by a circulation of ethylene glycol around copper jacketed walls, which allow a constant internal temperature to be maintained. LED arrays inside the volume provide ample illumination for high speed imaging in excess of 10 kHz. In typical operation the chamber is cooled to ~250 K, then opened to place a clean silicon wafer and droplet on the peltier cooler supported at the center of the volume. The solid state cooling element is then ramped to achieve a desired cooling or warming rate and subsequent operation proceeds in a completely automated fashion. A custom Labview interface is used to read the temperature inside the chamber. This system also controls the circulation chiller and solid state cooling element in the chamber. In order to distinguish the nucleation site in the freezing droplet, we use a post-trigger to save the data in the camera ring buffer. An IR thermocouple monitors the surface temperature of the droplet, and a software trigger is sent to the camera when a latent heat spike is observed as the droplet crystallizes. The IR thermocouple allows us to accurately determine the freezing temperature of each event.

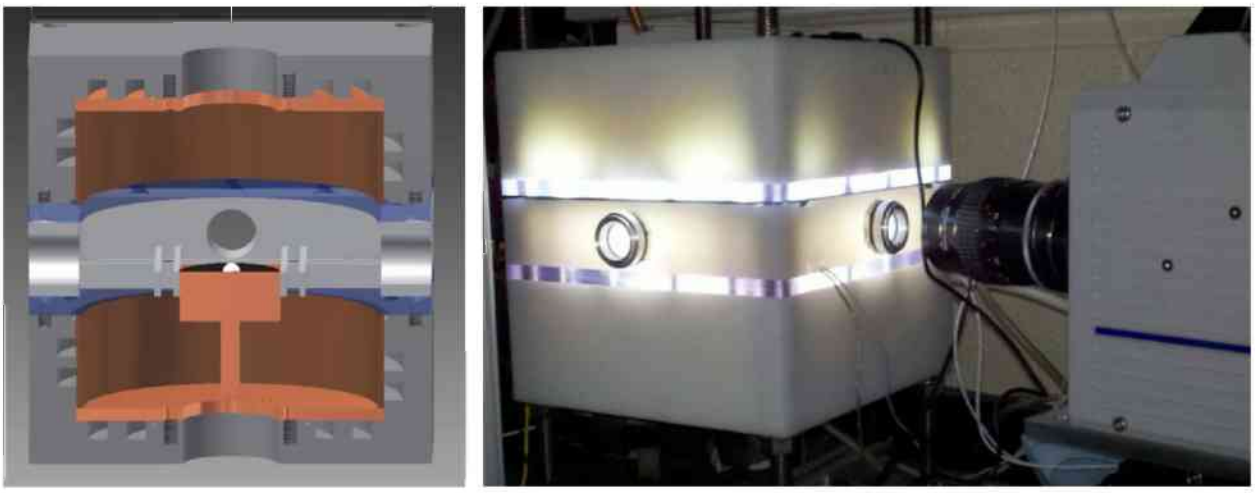

Figure 2.5: The left panel is a half cut schematic of the nucleation chamber. The test droplet is depicted as a white hemisphere resting on the dark silicon substrate. The right panel is an image of the actual chamber with a Photron SA2 camera arranged for horizontal imaging of a droplet in the middle of the chamber.

2.3 Investigation of the Influence of Contact Angle and Cooling Rate on Surface Crystallization

We carried out an investigation of surface crystallization as a pathway for heterogeneous ice nucleation. The experiments utilize the new environmental control chamber and two high speed cameras to image water drops freezing on a substrate. Experiments to investigate the role of contact angle and cooling rate on the freezing process have been carried out and one publication has resulted from that work. Experiments to study ice formation on microfabricated substrates are currently underway.

Recent experiments by Suzuki et al. (Chem. Phys. Lett. 2007, 445, 37−41) and Gurganus et al. (*J. Phys. Chem. Lett*. 2011, 2, 1449−1454) on liquid−solid nucleation arrived at conflicting results regarding a preferred status of the triple line between water, air, and an ice-catalyzing substrate. Temperature nonuniformity within drops and substrate-dependent contact angles have been suggested as culprits in a recent review by Sear (Int. Mater. Rev. 2012, 57, 328−356). To that end, we redesigned our earlier experiment to allow substrate-induced cooling and a side view with a second high-speed camera. The two camera views pinpoint the spatial location of nucleation sites in both the vertical and horizontal directions. Here we report such nucleation positioning results measured within drops freezing on a substrate. The role of thermal gradients was explored in three ways: (i) implementing direct cooling of the substrate; (ii) mimicking (higher) cooling rates used by Suzuki et al.; and (iii) varying the drop−substrate contact angle. No influence of thermal gradients on the preference for freezing at the triple line has been observed. Thermal simulations of the drop−substrate system confirm that horizontal temperature gradients are extremely small. Furthermore, treatment of the substrate to obtain a range of contact angles also yielded no preference for freezing at the triple line. The combined top and side views of the freezing drops suggest that apparent triple-line nucleation can be a spurious result of the viewing geometry. The results are explained in more detail in the following figures and their captions, as well as in the paper: Gurganus, C., A. B. Kostinski, and R. A. Shaw, 2013: High-speed imaging of freezing drops: Still no preference for the contact line. *J. Phys. Chem. C*, **117**, 6195-6200.

Figure 2.6: Pair of high-speed Photron SA2 cameras allows us to pinpoint nucleation sites and measure the droplet contact angle. In this film strip each frame represents a time step of 2 ms, or every 20th frame at a sample rate of 10 kHz. The nucleation site is evident at the center of the hexagonal crystal when the film is viewed in reverse.

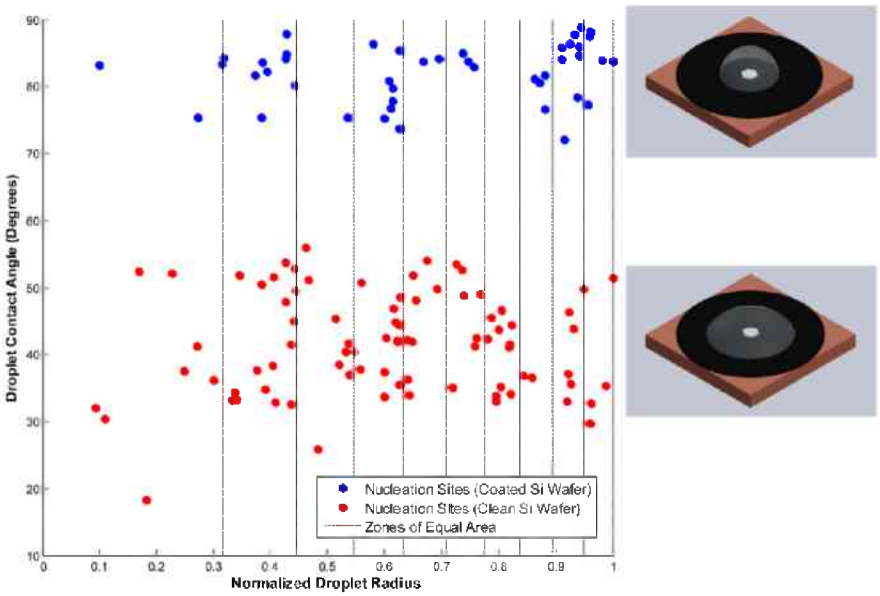

Figure 2.7: Image analysis from the side-view camera allows us to determine the contact angle of each droplet at the initiation of freezing. The red points indicate observed nucleation events on a clean Si wafer, while the blue points indicate observed nucleation sites on a silanized Si wafer. The dashed lines separate 10 zones on equal area to help guide the eye in the radial distribution of sites. The large variability in the observed contact angles of both sets is caused by pinning at the triple line during slow evaporation of the droplet. The approximate ranges for the observed drop contact angle, perimeter, and height are respectively 30−90°, 10−30 mm, and 1−2.5 mm. There appears to be no difference in the distribution of nucleation sites with contact angle.

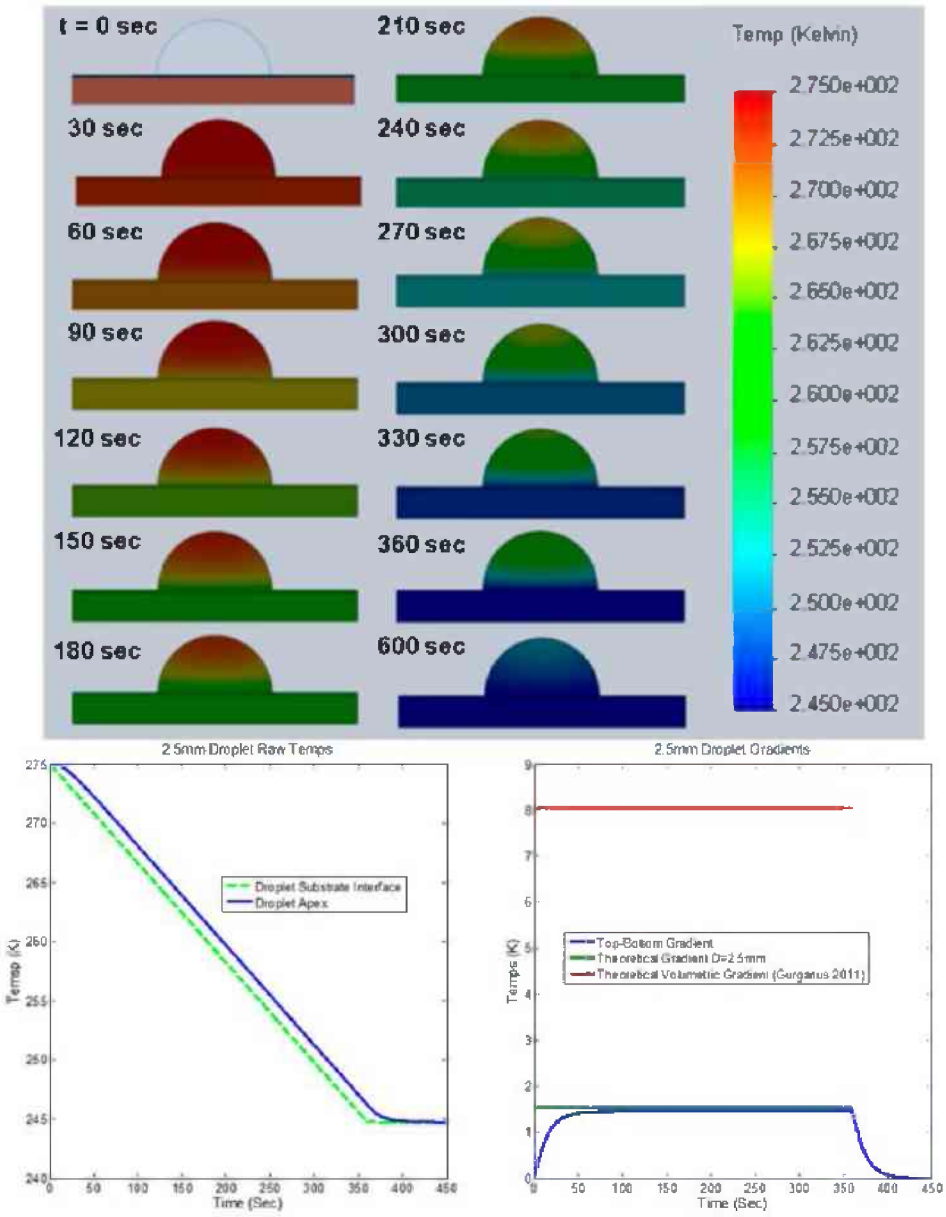

Figure 2.8: Results of our thermal analysis of this geometry using the Solidworks software package. This simulation mimics our experimental conditions, with the droplet, wafer, and heat sink initially at a stable equilibrium with the isothermal chamber (275 K). At t = 0, the temperature of the heat sink is decreased at a rate of 5 K/min for 360 s until it falls to a substrate temperature of 245 K, at which the temperature of the heat sink is held constant until the droplet comes into equilibrium. The bottom panels represent data from nodes at the top and bottom of the droplet. The first node is on the droplet−silicon interface. The selection of this bottom node is arbitrary because we observe no thermal gradient at the droplet−substrate interface. The second node is located at the apex of the droplet 2.5 mm above the interface. The left panel displays the raw temperature at both nodes during the cooling cycle. The right panel displays the thermal gradient that develops between these two nodes. After an initial transient stage (60 s), a steady state gradient of ~1.5 K is maintained throughout the cooling cycle. After the active cooling ends (360 s), the droplet relaxes exponentially toward the new equilibrium temperature.

2.4 Investigation of the Role of Surface Texture on Contact Nucleation

While nucleation of solids in supercooled liquids is ubiquitous, surface crystallization, the tendency for freezing to begin preferentially at the liquid-gas interface, has remained puzzling. Furthermore, in the presence of foreign catalysts the associated heterogeneous nucleation has been observed to prefer the three-phase contact line (triple line), especially for small particles and rough surfaces. Motivated by the conjectured importance of roughness and the contact line, we have searched for evidence of a shift to surface crystallization as the characteristic roughness length scale is decreased. Two plausible length scales associated with heterogeneous nucleation are: the critical radius for a nucleation seed, and $\delta \sim \tau/\sigma$, where τ is a relevant line tension and σ is the surface tension. These length scales range from nanometers to microns. We have found, using high speed imaging of the transient freezing process in supercooled water, that nano-scale texture causes a shift in the nucleation to the three-phase contact line, while micro-scale texture does not. Both the mean and variance of the freezing temperature are observed to increase, also pointing to the importance of nanotexture given that variances of independent causes add. The possibility of a transition or optimal length scale has implications for the effectiveness of nucleation catalysts, including formation of ice in atmospheric clouds.

Uniform probability of freezing is a standard assumption in nucleation theory: probability scaling as the volume of supercooled liquid for homogeneous nucleation, or as the area of the liquid–catalyst interface for heterogeneous nucleation. Recent studies suggest that for systems as widely varying as atomic liquids, salts, tetrahedral liquids, hexaourides, metal alloys, Nickel-Silicon, polymers, and water, homogeneous nucleation prefers the liquid-vapor interface, and therefore its rate scales not as volume but rather as area. The mechanism for surface crystallization remains unclear, and even more troubling, its predominance has been qualified and questioned. Meanwhile, experiments on the nucleation of ice on small particles in supercooled water have revealed a strong enhancement in nucleation rate for particles at the liquid-water – air interface, suggesting that whatever physics underlies surface crystallization likely extends to heterogeneous nucleation as well. Sorting out this mystery is more than academic because it addresses fundamental aspects of classical nucleation theory (CNT) and thus predictability of nucleation processes; some long standing puzzles such as the empirical observation that 'contact nucleation' is more efficient than 'immersion nucleation' in supercooled cloud droplets may well be intertwined with the physics of surface crystallization. A leading hypothesis for the preference for surface crystallization is the formation of a three-phase interface, and this aspect is investigated here for heterogeneous nucleation of ice in supercooled water.

The results are explained in more detail in the following figures and their captions, as well as in the paper: Gurganus, C. W., J. C. Charnawskas, A. B. Kostinski, and R. A. Shaw, 2014: Nucleation at the contact line observed on nano-textured surfaces. *Phys. Rev. Lett.*, accepted for publication (preprint available at http://arxiv.org/abs/1410.7640).

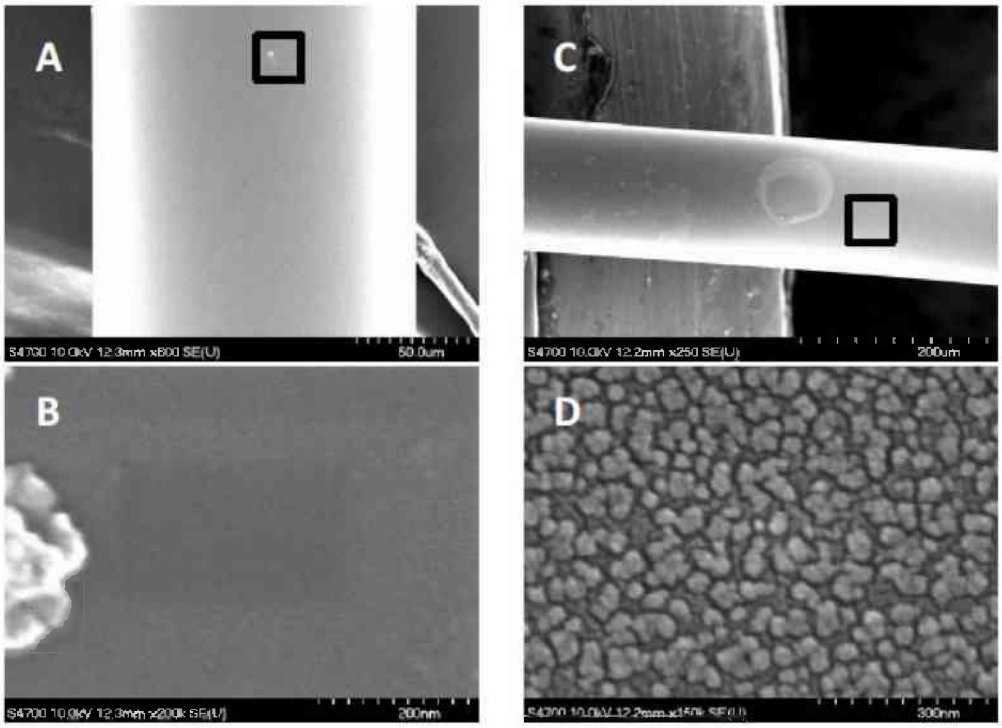

Figure 2.9: Fabricating surface texture spanning the range from 100 μm to 10 nm. Motivated by the conjectured importance of roughness to heterogeneous nucleation and the plausible range of length scales, these experiments were conducted with smooth optical fibers (A,B), nano-textured optical fibers (C,D), and micro-textured silicon substrates (not shown) as heterogeneous nucleation catalysts. Panels A-D were taken with a high resolution SEM.

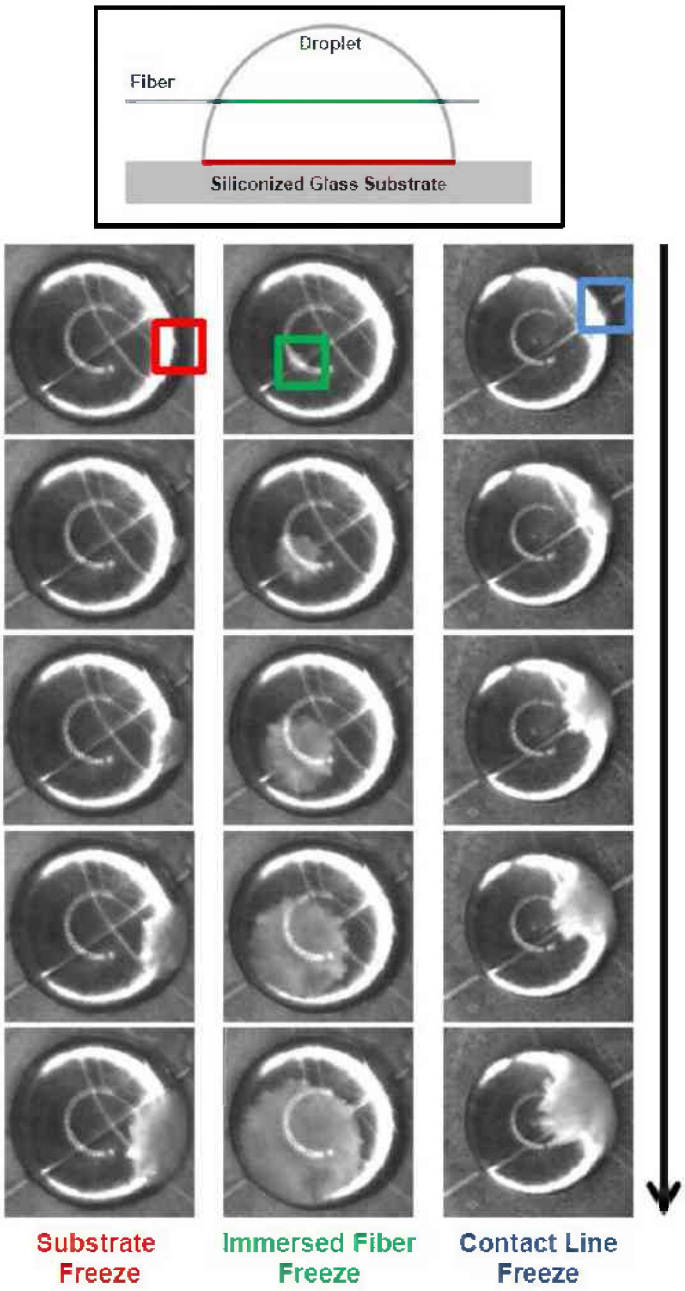

Figure 2.10: Three modes of nucleation Top: A schematic of the droplet-fiber geometry. A 30 µL droplet with a contact angle of ~ 90° rests on a siliconized glass slide (Hamilton Scientific) that is cooled from below (Gurganus et al 2013). An optical fiber, partially immersed within the droplet, can act as a heterogeneous nucleation catalyst. Three possibilities for nucleation then arise: on the substrate (red), on the immersed fiber (green) and at the fiber contact lines (blue). Bottom: By imaging the crystallization at 5 kHz we pinpoint the nucleation site (boxed area in film strips). Film strips here represent each of the three nucleation modes. Every 15th frame is shown resulting in a 3 msec spacing.

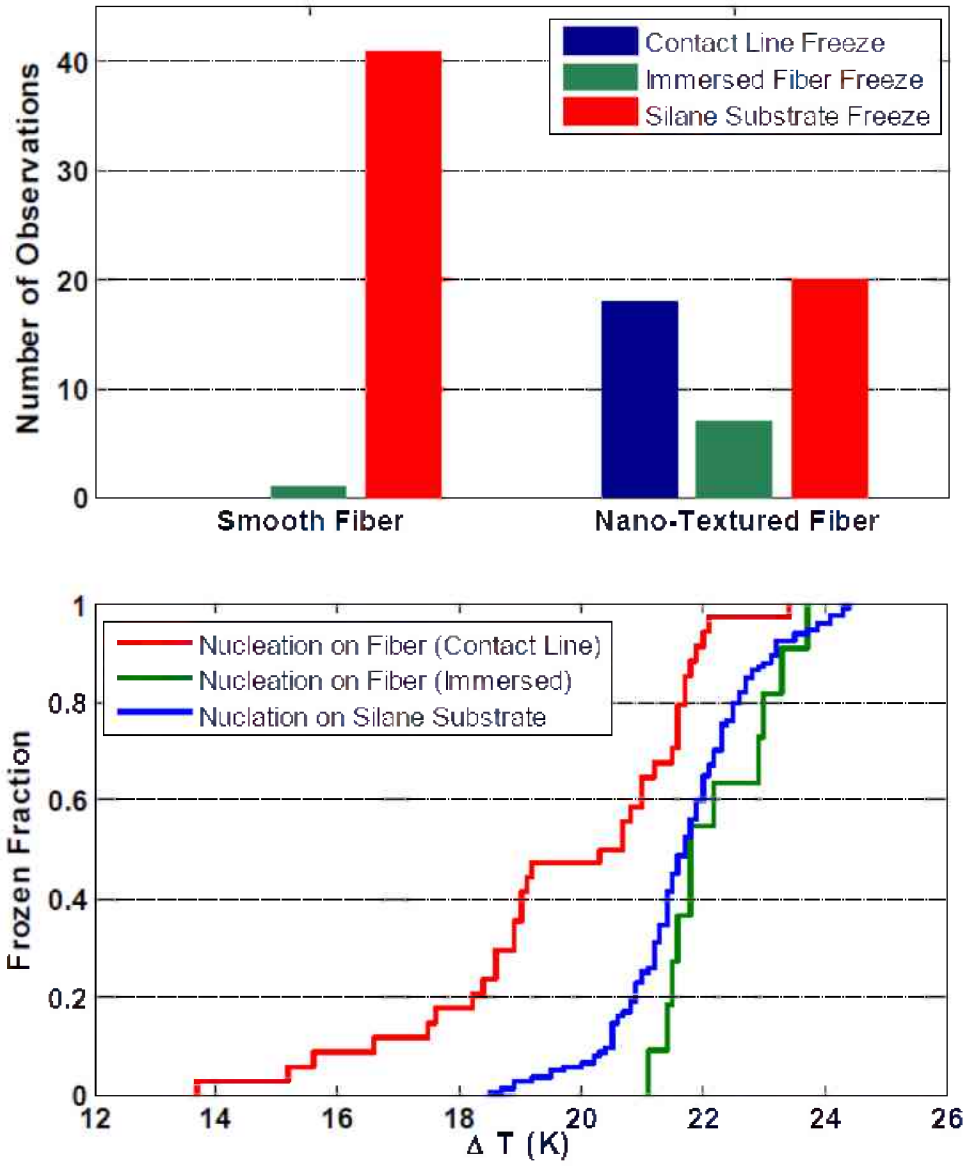

Figure 2.11: Nano-Texture observed to cause a transition to surface crystallization at the contact line. Results for the three modes of nucleation, substrate, immersed fiber, fiber contact line. Top Panel: Spatial origin of crystallization is observed often to shift to the contact line for nano-textured (rough) fibers, but neither the smooth fiber ($r = 70$ μm) nor the micro-textured substrates (2-100 μm, data not shown here) yield such a shift. Despite relatively small surface area of the nano-textured fiber, over half of freezing events are initiated there. Furthermore, despite the overwhelmingly small spatial odds, the majority of the fiber induced events originate at the contact line. Bottom Panel: Higher freezing temperatures (weaker supercooling) are observed for nucleation events at the fiber contact line as evidenced by the cumulative freezing probabilities (red curve). Broadening of the distribution accompanies fiber contact line events, as expected because of additional variability in the geometry of the nano-textured contact lines.

3. Electrodynamic Trap Nucleation Experiments

During this project we have developed a laboratory chamber able to suspend single aerosol particles in an environment with full thermodynamic control. The chamber is designed such that the suspended particle can be monitored continuously using direct imaging as well as light scattering methods. The goal is that with this chamber freezing of a single droplet, or deposition onto a single aerosol particle can be observed, as well as the subsequent growth. The figures that follow illustrate the chamber and its operating principle. To summarize, the chamber integrates two systems that have been used independently in prior work. First, a quadrupole particle levitation system allows individual charged aerosol particles, cloud droplets, or ice crystals to be suspended in the air, away from substrates or other surfaces. Second, a continuous flow system with cylindrical geometry with two wall-temperature regions allows an isolated region of supersaturation to be generated. As shown in the figures, the supersaturation region is designed to coincide with the location of levitated particles. With temperature differences between 0 and 10 K it is possible to achieve supersaturations over the full range of atmospherically relevant values. The current design uses several new engineering features: the quadrupole electrodes are outside of the flow tube, directly within the coolant, which allows for full isolation from the thermodynamic control.

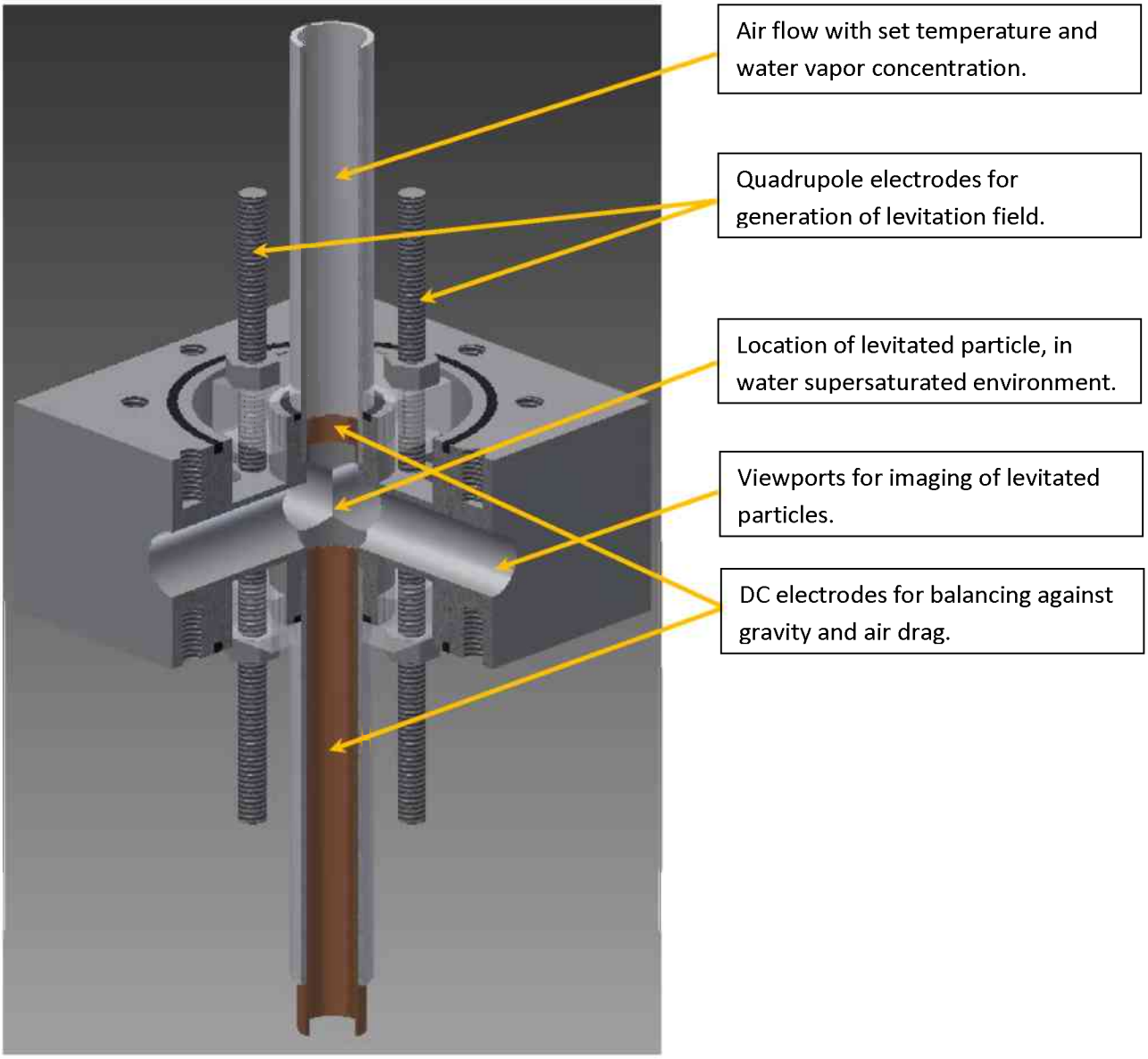

Figure 3.1: Schematic view of the new quadrupole particle trap with thermodynamic control. Four vertically oriented electrodes have high AC voltage applied for generating a quadrupole electric field in which one or more charged particles are levitated. Two DC electrodes generate a vertical field for counteracting air drag and gravitational forces acting on the particle. A continuous air flow along the vertically oriented tube sets the environment temperature and water vapor concentration. A step change in the temperature along the length of the tube wall allows a supersaturated environment to be externally controlled (see further details in the next figure).

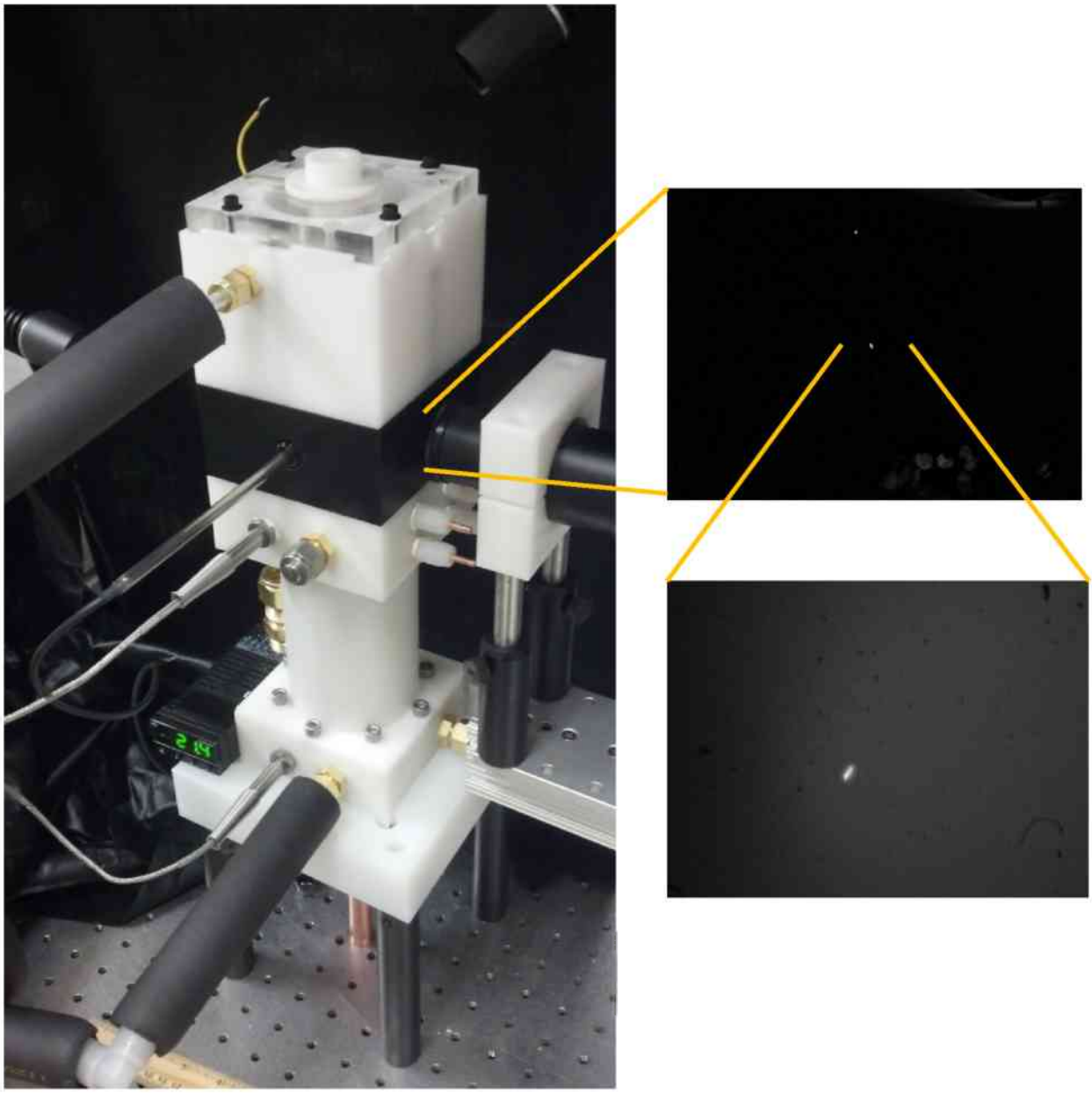

Figure 3.2: On the left is the quadrupole particle trap with supersaturation control. The black region in the center is where the quadrupole trap region is located, and the white sections are where the continuous-flow generation of supersaturation is located. On the right are two views of levitated cloud droplets. The top image is of two cloud droplets along the axis of the quadrupole field, with a separation distance between the droplets of several mm. The bottom image is a 7x magnification showing a slight orbit of the lower droplet.

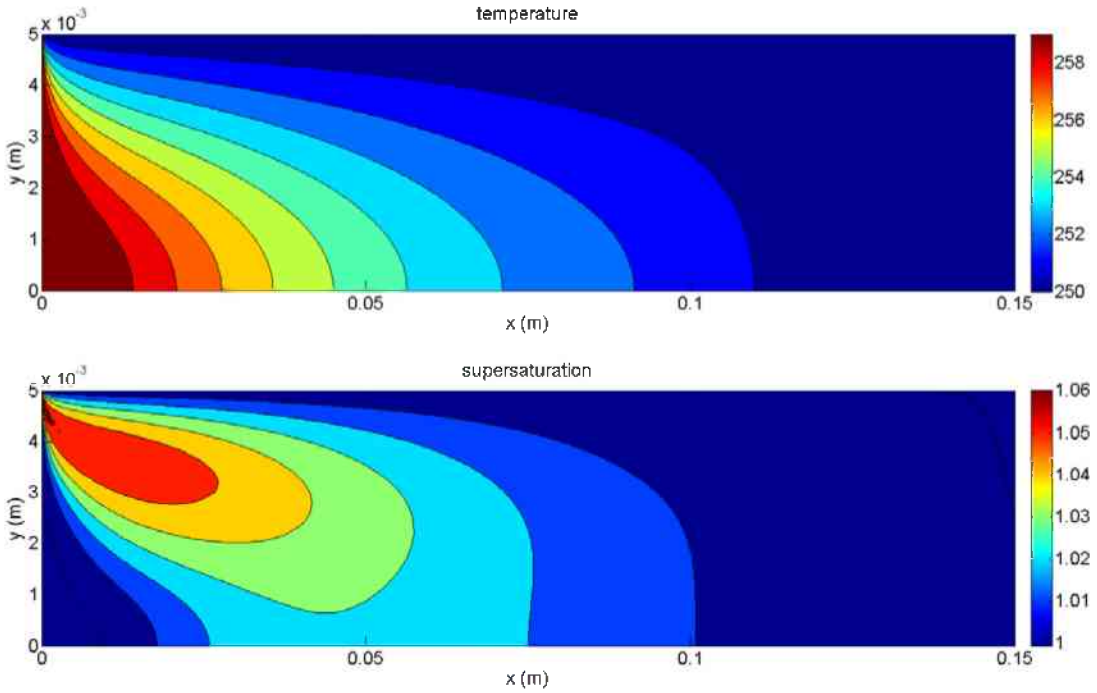

Figure 3.3: Results of a simulation of air flow through the cylindrical region inside the quadrupole levitation chamber. The contour plots are for an axisymmetric slice, with y representing the radius ($y = 0$ being the axis of symmetry) and x representing distance along the axis, with $x = 0$ being the region where the tube-wall temperature drops from 260 K to 250 K. The top panel shows contours of temperature and the entrance region where the air relaxes to the wall temperature can be clearly seen. The precise length of this entrance region is proportional to the flow speed, which can be adjusted. The bottom panel shows contours of supersaturation, which is generated as a result of the slightly difference between the thermal diffusivity and the diffusion coefficient for water vapor. For the flow speed simulated and the temperature difference of 10 K a peak supersaturation of approximately 2.5% is achieved along the axis of the tube, the region where levitated particles are located.

4. Nucleation and Ice Microphysics in Mixed-Phase Stratiform Clouds

Mixed-phase stratiform clouds can persist even with steady ice precipitation fluxes, and the origin and microphysical properties of the ice crystals are of relevance to radiative balances in polar and midlatitude regions. We have explored the question of whether persistent ice crystal precipitation from supercooled layer clouds can be explained by time-dependent, stochastic ice nucleation using an approximate, analytical model, and a large-eddy simulation (LES) cloud model. The updraft velocity in the cloud defines an accumulation zone, where small ice particles cannot fall out until they are large enough, which will increase the residence time of ice particles in the cloud. Ice particles reach a quasi-steady state between growth by vapor deposition and fall speed at cloud base. The analytical model predicts that ice water content (w_i) has a 2.5 power law relationship with ice number concentration n_i. w_i and n_i from a LES cloud model with stochastic ice nucleation also confirm the 2.5 power law relationship. The prefactor of the power law is proportional to the ice nucleation rate, and therefore provides a quantitative link to observations of ice microphysical properties.

The 2.5 power law described in the prior paragraph has been extended and made more general in subsequent work. Vapor deposition growth and sedimentation of ice particles along with a uniform volume source of ice nucleation lead to a power law relation between ice water content w_i and ice number concentration n_i with exponent 2.5. The result is independent of assumptions about the vertical velocity structure of the cloud and is therefore more general than the related expression of Yang et al. (2013). The sensitivity of the $w_i - n_i$ relationship to the spatial distribution of ice nucleation is confirmed by Lagrangian tracking and ice growth with cloud volume, cloud top, and cloud base sources of ice particles through a time-dependent cloud field. Based on observed w_i and n_i from Indirect and Semi-Direct Aerosol Campaign, a lower bound of 0.006 m^{-3} s^{-1} is obtained for the ice crystal formation rate.

The results are explained in more detail in the following figures and their captions, as well as in two published papers:

Yang, F., M. Ovchinnikov, and R. A. Shaw, 2013: Minimalist model of ice microphysics in mixed-phase stratiform clouds. *Geophys. Res. Lett.*, **40**, 1-5.

Yang, F., M. Ovchinnikov, and R. A. Shaw, 2014: Microphysical consequences of the spatial distribution of ice nucleation in mixed-phase stratiform clouds. *Geophys. Res. Lett.*, **41**, 5280-5287.

This work has been carried out in collaboration with Dr. Mikhail Ovchinnikov at PNNL and the work will continue by comparing the theoretical expressions to more detailed LES cloud model results, as well as to ISDAC and M-PACE measurements of ice water content and ice number density. A primary motivation of this work is to have a relatively simple, analytical model that can serve as a bridge between highly detailed laboratory measurements of ice nucleation processes, and the kinds of microphysical variables that are observable through ARM and in situ measurements.

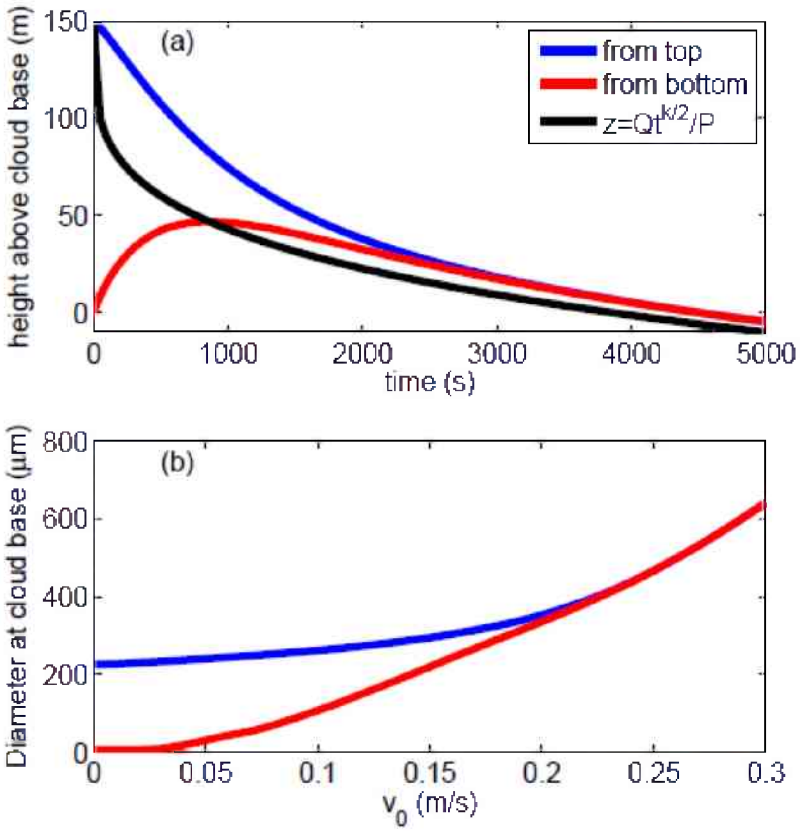

Figure 4.1: (a)Height of ice particle above cloud base vs time. Updraft velocity decreases linearly from $v_0 = 0.3\ m/s$ at the base to zero at the top. Blue line represents ice formed at cloud top, red at cloud base. Black line is based on quasi-steady state (Eq. 2). (b) Diameter at cloud base of ice particles which forms at cloud top (blue) and cloud base (red) under different background updraft velocity v_0.

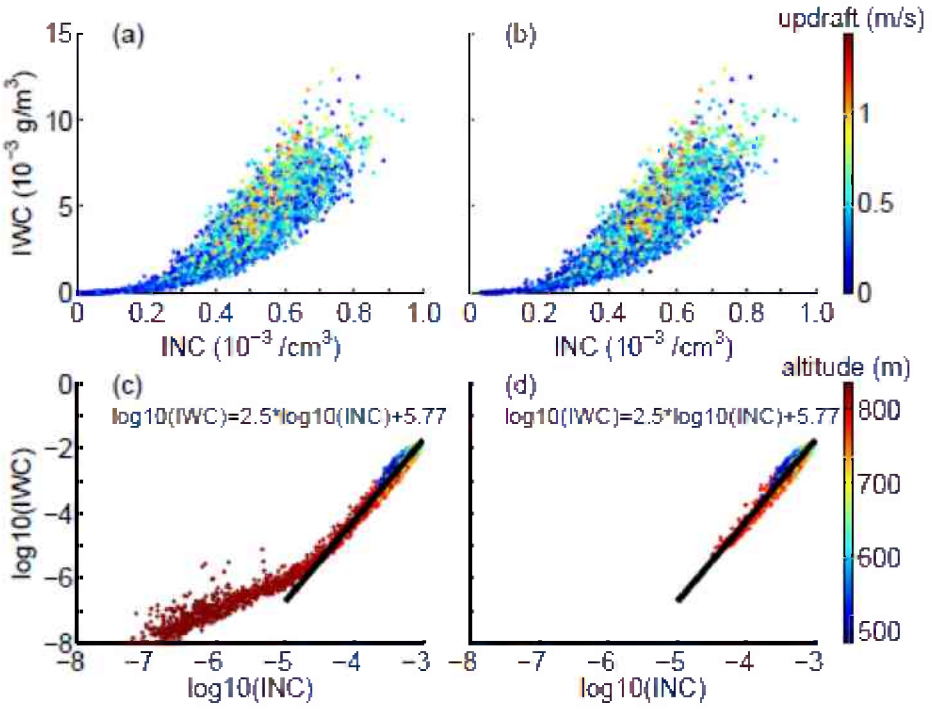

Figure 4.2: Ice water content and ice number concentration relationship from LES. (a) and (c) are accumulation zone region. (b) and (d) are selective accumulation zone region. Black lines in (c) and (d) are best fitted 2.5 slope lines. Colors in (a) and (b) represent updraft velocity, while colors in (c) and (d) mean altitude. The cloud base and top are at about 600 m and 800 m, respectively.

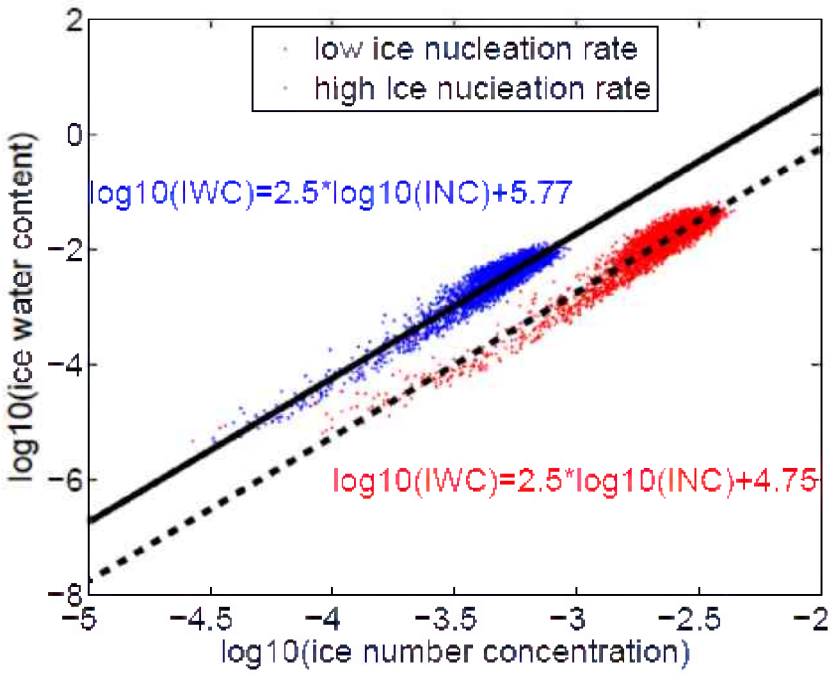

Figure 4.3: w_i and n_i relationship for two ice nucleation rates. Blue points are from LES with a nucleation rate of 2×10^{-9} and red points with a nucleation rate of 1×10^{-8}. Solid and dashed lines are best fitted 2.5 slope lines, and the difference in the intercepts is quantitatively explained by the difference in nucleation rates.

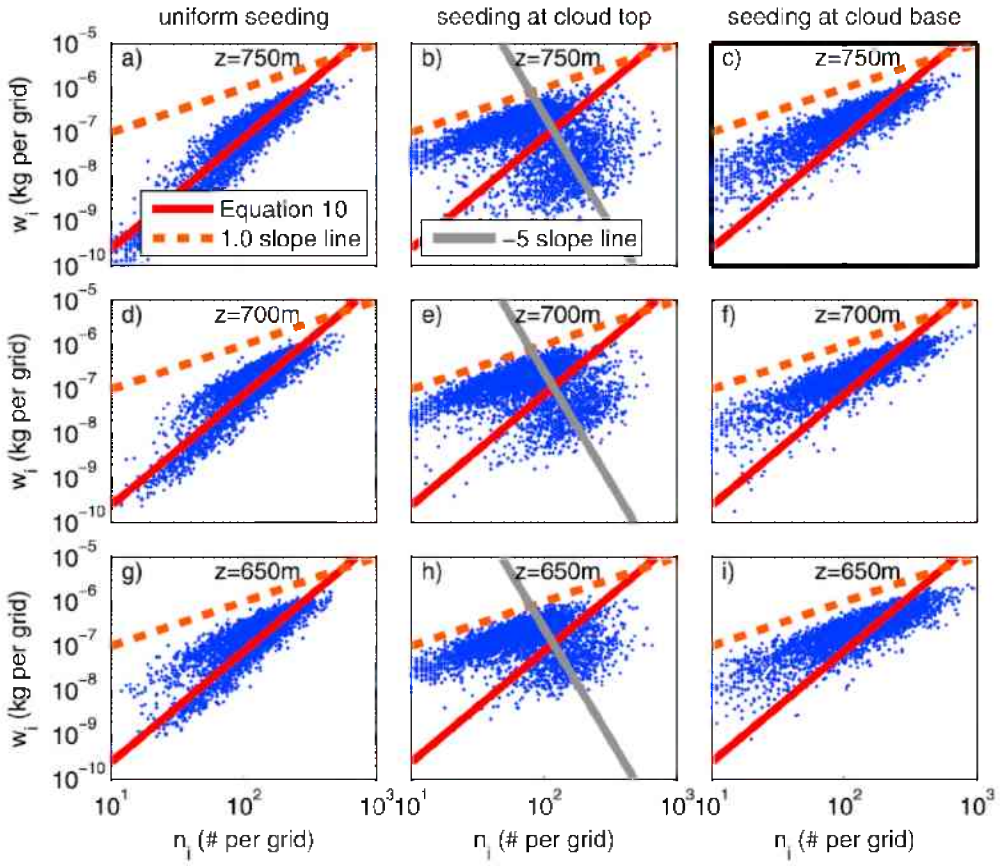

Figure 4.4: w_i versus n_i relationship at three different heights within the cloud, and for three different ice nucleation ("seeding") geometries. Top, middle, and bottom rows are 750 m, 700 m, nad 650 m, respectively. The left column is for ice nucleation distributed uniformly throughout the cloud volume. The middle column is for ice nucleation occurring at cloud top, and the right column is for ice nucleation occurring at cloud base. Blue points are values observed at LES grid points at the specified height. The dashed red line has a power law exponent of 1.0, corresponding to simple mixing or dilution. The solid red line has a power law exponent of 2.5, as predicted for spatially uniform, steady ice nucleation rate. The grey line has a power law slope of -5, as predicted for ice nucleation at cloud top.

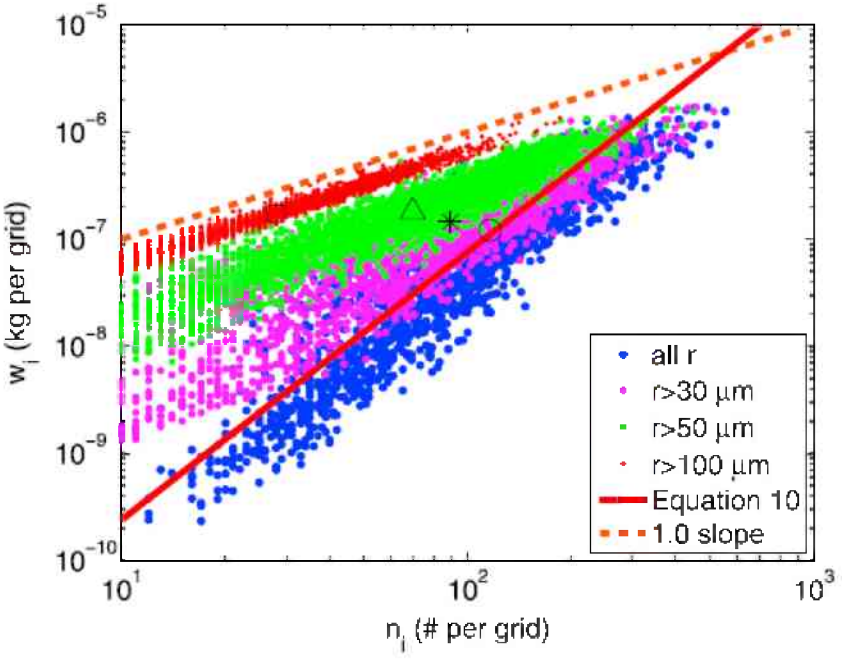

Figure 4.5: w_i versus n_i relationship for different threshold radii from the Lagrangian particle tracking model. The red line is calculated from the theory for uniform nucleation rate, and the dashed line, shown for comparison, has a 1.0 power law exponent. As the threshold radius is increased, the simulated measurements steadily lose the predicted 2.5 power law exponent.